PAPER • **OPEN ACCESS**

Surface-process correlation for an ink-jet printed transparent fluoroplastic

To cite this article: Carlos Gomez *et al* 2020 *Surf. Topogr.: Metrol. Prop.* **8** 034002

Surface Topography: Metrology and Properties

OPEN ACCESS

RECEIVED
27 April 2020

REVISED
4 June 2020

ACCEPTED FOR PUBLICATION
4 August 2020

PUBLISHED
20 August 2020

PAPER

Surface-process correlation for an ink-jet printed transparent fluoroplastic

Carlos Gomez[1], **Carlo Campanelli**[2], **Rong Su**[1] **and Richard Leach**[1]

[1] Manufacturing Metrology Team, Faculty of Engineering, University of Nottingham, United Kingdom
[2] Centre for Additive Manufacturing, Faculty of Engineering, University of Nottingham, United Kingdom

E-mail: carlos.gomez@nottingham.ac.uk

Keywords: additive manufacturing, ink-jet printing, surface topography, metrology, coherence scanning interferometry, surface-process correlation, THV fluoropolymer

Abstract

Ink-jet printing is one of the key technologies in the field of defined polymer deposition. There is currently a lack of knowledge regarding how some fluoropolymers, in this case THV 221, can be ink-jet printed. A quantitative analysis of the micro-scale areal surface topography measured with coherence scanning interferometry can advance the understanding of the correlation between the ink-jet printing process and the resulting surface topography. Our experimental design covers a variety of ink-jet printed THV 221 structures with basic geometric shapes such as dots and films, ranging from a few nanometres to tens of micrometres in height, and from tens of micrometres to a few millimetres in spatial wavelength. Relevant printing parameters, including polymer concentration, drop spacing and number of layers have been selected and varied to produce the samples used for the study. This investigation also provides an insight into how to control and optimise the quality of THV 221 printed parts.

1. Introduction

Additive manufacturing (AM) [1] techniques provide additional options to engineering, biomedical and architecture industries, amongst others, and significant advantages for specific applications, such as the fabrication of polymer electronics and microlenses [2, 3], relative to conventional manufacturing processes. This is mostly because AM allows the creation of complex geometries and internal features that cannot be produced using subtractive methods due to their inherent tool path restrictions, or without the need of moulds as in formative methods [1]. AM technologies are currently able to fabricate parts made of metals, ceramics and polymers, the latter being the most widely used material class in AM [3].

Ink-jet printing is an AM process where droplets of feedstock material (i.e. solution or ink) are selectively ejected with precise coordinates and amounts to form a final product or part [1]. Typically, ink-jet printing means printing a two-dimensional (2D) document or image, meanwhile in AM refers to the printing of three-dimensional (3D) parts or structures by printing multiple layers [4, 5]. Given that polymers are most suitably processed from solution, ink-jet printing is considered to be one of the key technologies in the field of defined polymer deposition [5].

AM parts in general, have suffered until recently from a lack of understanding of the mechanisms of the underlying processes [6]. The measurement and characterisation of surface topography can allow a manufacturer to better understand how the features of a given topography were formed, and ultimately how these features relate to the manufacturing process that created that surface [7, 8].

There is scarce knowledge regarding how some fluoropolymers, in this case THV, can be ink-jet printed [9, 10]. A quantitative analysis of the micro-scale areal surface topography can provide a better understanding of the characteristic textures that result from the ink-jet printing process of this polymer. Most THV applications include multilayer parts, where a thin layer can be used as a protective coating or to provide enhanced barrier properties to other layers [9, 10]. The demand for nanometre-thick films is constantly increasing and ink-jet printing can address this level of miniaturisation due to its high resolution and precision [3].

In this work, we carried out an investigation into the characteristics of the topography of ink-jet printed

THV 221 surfaces. We ink-jet printed several THV 221 samples that cover a variety of structures with basic geometric shapes, such as dots and films. The sizes of the polymer structures ranged from a few nanometres to tens of micrometres in thickness (i.e. height), and from tens of micrometres to a few millimetres in spatial wavelength (i.e. lateral width). To produce the polymer structures, we selected and varied relevant printing parameters, which included the polymer concentration, drop spacing and number of layers.

The goal of the present work is to assess the feasibility of ink-jet printing THV 221 and to provide a better understanding of the features and characteristic textures that result from the ink-jet printing process. This paper provides an insight in to how to control and optimise the quality of THV ink-jet printed parts.

2. Materials and methods

2.1. THV 221

THV 221 is a transparent fluoroplastic comprised of 51.4% tetrafluoroethylene (TFE), 10.4% hexafluoropropene (HFP) and 38.2% vinylidene fluoride (VDF) [11]. Fluoroplastics are polymers with multiple carbon-fluorine bonds [12]. This family of polymers have been widely used in the automotive, electrical and chemical industries, as well as in medical devices and aircrafts [13, 14], since their properties allow wide service temperatures and high resistance to chemicals, sunlight, flames and weathering. Fluoroplastics are probably most recognised for their use as a coating for non-stick cookware, i.e. polytetrafluoroethylene (PTFE) or for insulating wire and cable [14].

Despite the relatively low melting temperature of 115 °C, the decomposition temperature of THV 221 is around 410 °C [11]. The properties of THV include high transparency, bondability to itself and other substrates, high flexibility, low flammability, high chemical and permeation resistance, low refractive index as well as efficient electron beam cross-linking [9, 13].

Most THV applications include multilayer parts, where a thin layer is used as a protective coating or to provide enhanced barrier properties to other layers [10]. The THV film formation processes, such as drop casting and electrospinning, are described elsewhere [11, 15]. THV has been used in medical applications, such as for coronary stents [16], due to its high biocompatibility and low drug permeability. THV can also be used in microfluidic devices due to its transparency, thermal resistance and chemical resistance [17, 18].

Ink-jet printing can benefit existing and potential applications that require miniaturisation due to its high resolution and precision (the smallest achievable resolution depends on the drop size, which is normally around 50 μm [19]). The literature about the ink-jetting of fluoropolymers is relatively limited and mainly focused on polyvinylidene fluoride (PVDF) [20, 21]. With the exception of PTFE and polyvinyl fluoride (PVF), all fluoropolymers are melt processable [13] but only a few are soluble in common solvents at room temperature, such as PVDF and THV 221 (THV is available in several grades but only THV 221 is soluble in conventional solvents [11]).

Table 1. Vapour pressure and viscosity at 20 °C for the solvents used to dissolve THV [24].

Solvent	Vapour pressure/ mmHg	Viscosity/ (mPa·s)	Boiling temperature/°C
Acetone	184.5	0.4	56.3
Ethyl acetate	73.0	0.5	77.1
MIBK	16.0	0.6	117.4
DMAc	1.3	2.1	166.1

Table 2. Viscosity of THV 221 inks (mean of three measurements) at different temperatures.

THV 221 formulation	Viscosity/mPa·s		
	22 °C	35 °C	45 °C
1 wt% in MIBK	0.9	0.8	—
10 wt% in MIBK	73.3	44.7	36.1
20 wt% in 50–50 vol% in MIBK–acetone	1088.0	848.8	680.1

2.2. Ink-jet printing of THV 221

Fujifilm Dimatix™ DMP-2850 [22] and Nordson EFD PICO Pμlse® [23] ink-jet deposition systems were used to print the THV 221 inks on glass substrates. The printers were located in a laboratory with a controlled temperature of (21.0 ± 1.0) °C. Printer settings such as waveform, frequency and jetting voltage were adjusted following the manufacturer's guidelines.

As ink-jet printing requires relatively low viscosities, polymers can only be deposited from dilute solution [5]. Common solvents used to dissolve THV are acetone, ethyl acetate, methyl isobutyl ketone (MIBK) and dimethyl acetamide (DMAc) [16] (see table 1). MIBK was selected as the main solvent because of its vapour pressure, which would allow a fast evaporation of the THV 221 inks, but not so fast that it could lead to blockages in the nozzles of the printers.

The shear viscosity of the formulated THV 221 inks was measured using a rheometer at a shear rate of 100 s^{-1} (see table 2). The shear viscosity for inkjet applications is usually measured at a shear rate of 100 s^{-1} as standard rheometers cannot reach the actual shear rates of jetting [4, 19]. In this paper, the polymer concentration of the inks is expressed in weight percent (wt%) and the solvent ratio is expressed in volume percent (vol.%).

Due to the relatively high polymer concentration of the THV 221 20 wt% ink, acetone was added to MIBK at a 1:1 ratio by volume (i.e. 50–50 vol% MIBK–acetone) to enhance dissolution. The THV 221 1 wt% in MIBK ink was printed using the Dimatix system

Table 3. CSI instrument specification.

Magnification	5.5×	20×
Numerical aperture	0.15	0.40
0.5 × zoom lateral sampling distance/μm	2.95	0.82
1 × zoom lateral sampling distance/μm	1.47	0.41
0.5 × field of view/mm	3.02 × 3.02	0.84 × 0.84
1 × field of view/mm	1.50 × 1.50	0.42 × 0.42

with a nominal nozzle diameter of 21 μm and a nozzle temperature of 28 °C, which corresponds to the minimum adjustable nozzle temperature of the printer.

The THV 221 10 wt% in MIBK and the THV 221 20 wt% in 50–50 vol% MIBK–acetone inks were printed using the PICO Pμlse system with a nominal nozzle diameter of 150 μm and a nozzle temperature of 30 °C and 50 °C, respectively. The PICO printer allows the jetting of inks with higher viscosities.

We ink-jet printed single and multiple layers of dots and films. The thickness of the printed parts range from a few nanometres to tens of micrometres.

2.3. Surface-measuring coherence scanning interferometry

Coherence scanning interferometry (CSI) is a non-contact optical technique for measuring areal surface topography with sub-nanometre measurement noise [25]. The detailed working principle of CSI can be found elsewhere [26–29]. CSI can measure a variety of surface types [28, 29], including applications that incorporate the measurement of AM parts [30], as well as transparent film structures and dissimilar materials [31, 32]. CSI has been used for the quality assurance of ink-jet printed polymer layers of drug-delivery systems [33] and for the characterisation of polymer coatings in silicon micro-electromechanical systems [34].

CSI has the advantage of being faster than contact methods and has been selected for this application since it can measure transparent materials with high precision and without any potential damage to the investigated surfaces [28]. It has been identified elsewhere that contact stylus measurements are liable to damage polymer surfaces [35].

A Zygo NewView™ 8300 CSI system was used in this work. The instrument was located in a metrology laboratory with a controlled temperature of (20.0 ± 0.5) °C. The specifications of the employed objective lenses are shown in table 3.

An objective lens with a lower magnification and zoom provides a larger field of view (FOV) but a lower lateral resolution [36]; however, a larger FOV is convenient when measuring the ink-jet printed surfaces because form information can be obtained without using stitching of many single measurements. A lens with a high numerical aperture (NA) is useful when the surface contains steep slopes that can cause a reduction of the intensity of the interferometric signal and consequently result in lost data points, or when high-resolution local details of the surface topography are desired [28].

Dynamic noise reduction was enabled to enhance the signal-to-noise ratio (SNR) as the material is transparent [28, 37]. By using dynamic noise reduction, the number of valid topography data points can be significantly increased [25, 30].

2.4. Surface topography analysis

The thickness calculation was performed in a commercial surface analysis software [38], in a similar way to the calculation of a step height, using the following method. The central thickness T_c for each investigated ink-jet printed THV sample was determined as the height difference between the mean height values of the top surface $\bar{h}_{top}$ (central region) and the glass substrate surface $\bar{h}_{glass}$. The topography data was levelled by subtracting the mean least-squares plane corresponding to the glass substrate surface. In a following step, an area of (100 × 100) μm around the centre of the top surface of the sample was selected and then a horizontal plane was obtained by averaging the height values located within the selected area. Similarly, a second horizontal plane was defined by the mean surface height value corresponding to the glass substrate. T_c was then calculated as the axial distance between these two parallel planes:

$$T_c = \bar{h}_{top} - \bar{h}_{glass}. \quad (1)$$

The edge thickness T_e of the printed drops was estimated as the height difference between the mean height value of the peaks localised at the edge of the drops $\bar{h}_p$ (this feature will be described in the following section) and the glass substrate:

$$T_e = \bar{h}_p - \bar{h}_{glass}. \quad (2)$$

In this study, we did not use the film measurement method described in [31, 32] to calculate thickness, instead, thickness was measured like a step height (see figure 1). We took the latter approach because the film measurement method requires accurate information of the refractive index of the films, otherwise measurement uncertainty could be increased. Furthermore, the measurement of edge thickness (T_e) may not be possible using the film measurement method as the edges are essentially thin walls.

For the printed drops, the variation of T_c and T_e was considered by measuring ten samples and then calculating the standard deviation, respectively. For the printed films, the variation of T_c was estimated as the standard deviation of five results (where each result corresponds to a different measured sample).

The surface texture of the ink-jet printed THV films was evaluated using the areal surface texture parameter *Sq* [39]—the root mean square surface height deviation within a defined area. Levelling was

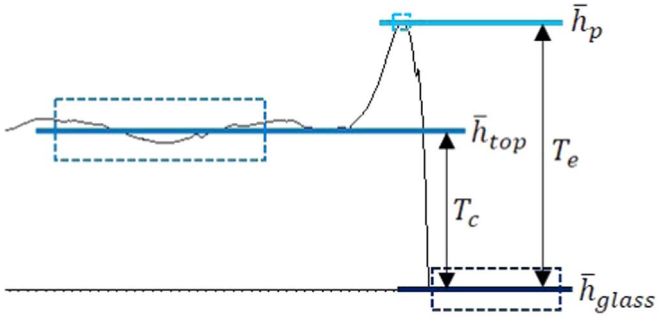

Figure 1. Diagram of thickness calculation.

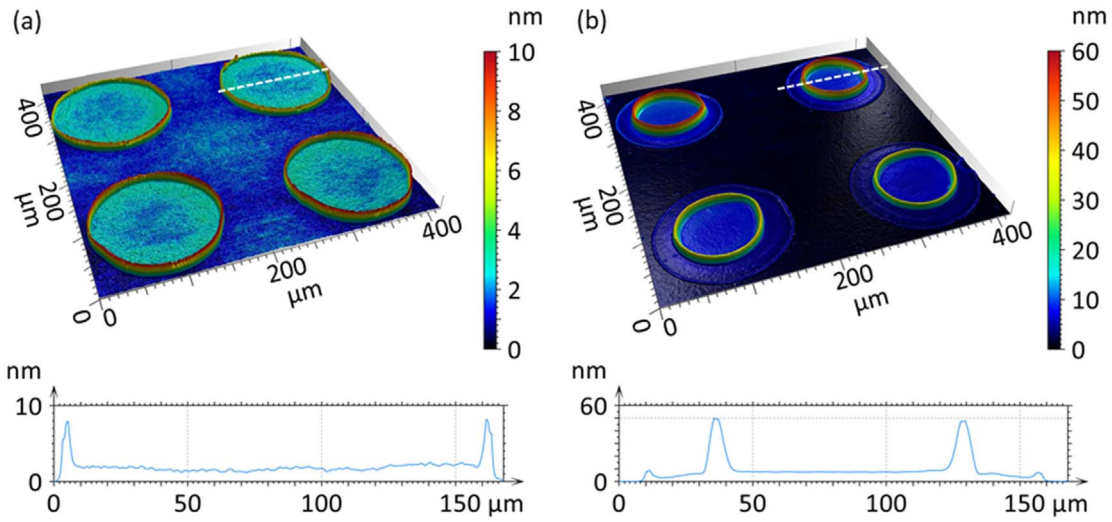

Figure 2. Surface topography and profiles corresponding to (a) one and (b) two-layer ink-jet printed drops of THV 1 wt% in MIBK.

applied using least-squares mean plane subtraction. An S-filter with a nesting index of 2.5 μm and an L-filter with a nesting index of 250 μm were applied to remove high-spatial frequency noise and long-scale waviness/form [40].

3. Results

3.1. THV 1 wt% in MIBK

Single-layer drops of THV 1 wt% in MIBK formed nanometre thickness films that showed polymer accumulation at the edges (see figure 2(a)), having $T_c = 2$ nm and $T_e = (8 \pm 2)$ nm (T_c is the central thickness and T_e is the edge thickness, estimated using equations (1) and (2), respectively).

The observed polymer accumulation at the edges of the drops is the result of a phenomena known as the 'coffee ring effect' [41, 42], and refers to the solutes or dispersed particles in a solution that accumulate at the perimeter of an evaporating drop (or film), caused by outward capillary flows due to uneven solvent evaporation rates. The higher amount of solute at the edge or perimeter causes the formation of a ring that can be significantly thicker than the centre of the evaporated drop [42]. In the absence of the coffee ring effect, the solutes of an evaporating drop are evenly distributed, resulting in a uniform thickness.

Two-layer drops of THV 1 wt% in MIBK (see figure 2(b)) showed $T_c = (8 \pm 1)$ nm and $T_e = (50 \pm 9)$ nm. In this case, two edges were present, where the higher edge corresponded to the double-layer drop, which had a smaller width than the single-layer drop.

The observed decrease in drop width while printing on a previous layer is caused by a higher contact angle of the THV 1 wt% in MIBK ink when it is deposited on a THV coated glass substrate, which was $(60 \pm 0.5)°$, relative to when the ink is deposited on an uncoated glass substrate, which was $(18 \pm 1.4)°$. The contact angle was determined by pendant and sessile drop analysis at a room temperature of 22 °C, considering the mean value and standard deviation of five repeated measurements. The contact angle is defined as the angle between the substrate surface and the tangent at the edge of the droplet's ovate shape, and it provides a measure of the ability of the ink to wet the surface of a substrate [43].

The thickness evolution with increased number of layers of the ink-jet printed drops of THV 1 wt% in

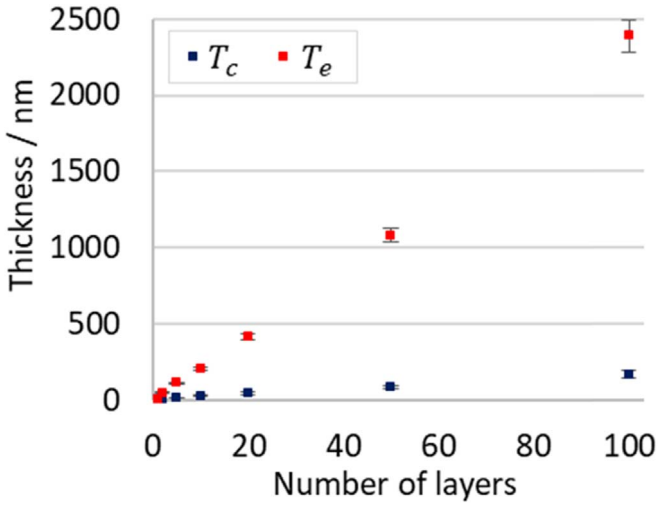

Figure 3. Thickness for the centre (T_c) and edge (T_e) of ink-jet printed drops of THV 1 wt% in MIBK with increased number of layers.

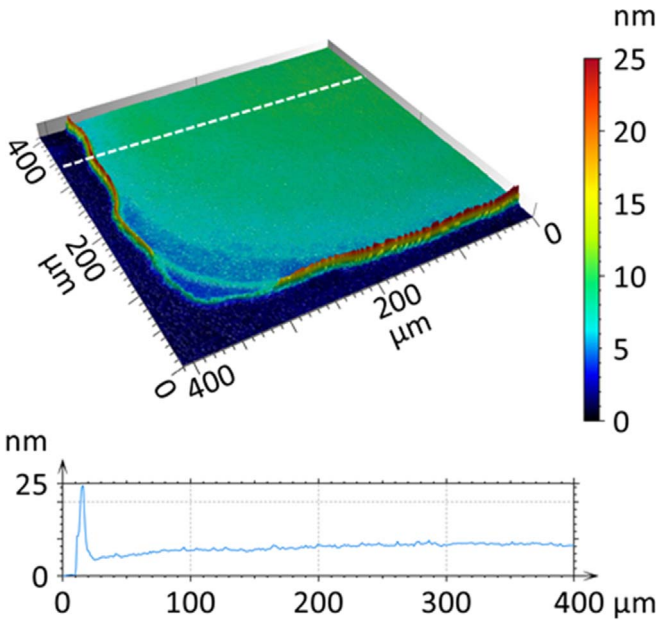

Figure 4. Surface topography and profile of a one-layer ink-jet printed film of THV 1 wt% in MIBK.

MIBK is shown in figure 3. The thickness at the edges of the drops (T_e) increased at a ratio that was approximately ten times greater than the increase ratio at the centre (T_c).

Single-layer films were printed at drop spacings of 60 μm, 80 μm, 100 μm and 120 μm. The highest-quality results were obtained with a drop spacing of 80 μm, which generated smooth and uniform films, as shown in figure 4. The films had $T_c = (8 \pm 1)$ nm, with $Sq < 1$ nm calculated over an area of (300×300) μm at the centre of the film.

Multiple layers were printed with a drop spacing of 80 μm, however, unexpected topography patterns started to appear. To further investigate the cause of the observed topography patterns, drop spacings of 100 μm and then 120 μm were used to print 2, 5, 10, 20 and 50 layers.

With a drop spacing of 100 μm, bump-like features appeared between the positions of the jetted drops after the second layer. The formation of the bumps was counterintuitive as they did not form in the centre of the printed drops, instead, they formed in between the drops. This effect was likely caused by the coffee ring effect. After 5 layers, the bumps increased in size, as shown in figure 5(a), and after 10 layers, the bumps became smoother and partially joined together with the neighbouring bumps, forming craters with the shape of the drops (see figure 5(b)). After 20 layers, the bumps fully joined together, and the craters became well defined (figure 5(c)). After 50 layers, the

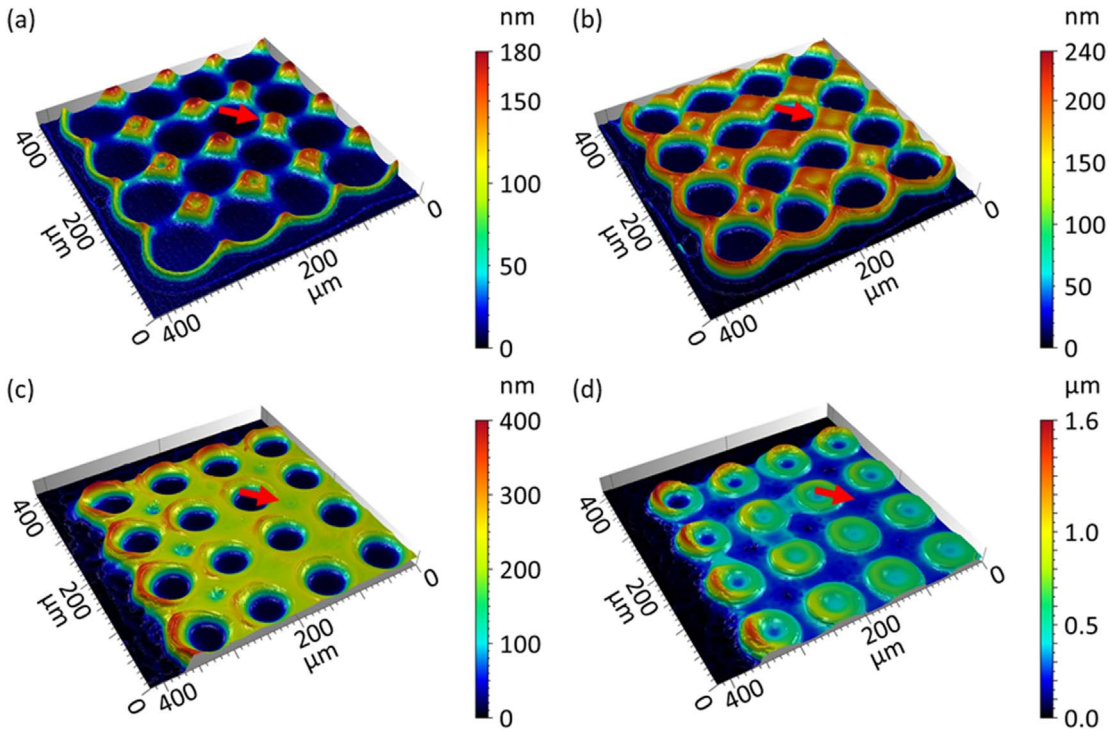

Figure 5. Surface topography corresponding to (a) five-layer, (b) ten-layer, (c) twenty-layer and (d) fifty-layer ink-jet printed films of THV 1 wt% in MIBK.

craters were higher than the regions between the jetted drops (figure 5(d)).

When a drop spacing of 120 μm was used, a similar trend was observed, but in this case, the drops did not touch as much as in the previous case. Peaks were formed by the overlapping regions of the contours of neighbouring drops likely caused by the coffee ring effect. With a smaller drop spacing the peaks would join in the centre between neighbouring drops, explaining the formation of bumps observed with a drop spacing of 100 μm.

3.2. THV 10 wt% in MIBK

The optimal nozzle temperature for ink-jet printing THV 10 wt% in MIBK was 30 °C, as splashing was observed with higher nozzle temperatures. The coffee ring effect was present when drops where printed, as can be observed in figures 6(a), (b), nevertheless, the effect was not as strong as in the case of THV 1 wt% in MIBK.

Single-layer drops of THV 10 wt% in MIBK had $T_c = (1.52 \pm 0.11)$ μm and $T_e = (2.40 \pm 0.20)$ μm. Double-layer drops gave $T_c = (2.29 \pm 0.21)$ μm and $T_e = (5.61 \pm 0.31)$ μm. The decrease in drop width on the second layer was consistent with the observed results for the THV 1 wt% in MIBK ink, which is explained by the difference in the contact angle with different substrate surfaces, i.e. uncoated glass or THV coated glass.

Films of THV 10 wt% in MIBK were ink-jet printed using a drop spacing of 500 μm (approximately 20% of overlapping). The printed films did not show the coffee ring effect, as can be observed in figures 6(c), (d). The measured surface topographies of the films exposed the presence of a slipping pattern towards the edges, likely caused by the non-pinning of the film edge on the substrate.

Single-layer films had $T_c = (3.53 \pm 0.29)$ μm, showing a texture of $Sq = (40 \pm 5)$ nm. Double-layer films had $T_c = (7.21 \pm 0.60)$ μm and $Sq = (729 \pm 186)$ nm, and showed the presence of wrinkle-like features on the surface. Sq was calculated over an area of (1×1) mm at the centre of the films. The wrinkle-like features were likely formed by the swelling of regions of the underlying THV film during the drying process, followed by a sudden and violent expansion of poorly dissolved regions [44, 45].

3.3. THV 20 wt% in 50–50 vol% MIBK–acetone

The optimal nozzle temperature for ink-jet printing THV 20 wt% in 50–50 vol% MIBK–acetone was found to be 50 °C, as higher temperatures caused splashing, while lower temperatures decreased splashing but made the ink-jetting process less reliable (e.g. faulty drop ejection).

The coffee ring effect was almost absent for the case of the ink-jet printed drops, as can be observed in figures 7(a), (b). Single-layer printed drops of THV 20 wt% in 50–50 vol% MIBK–acetone had $T_c = (5.91 \pm 0.21)$ μm and $T_e = (6.40 \pm 0.21)$ μm. Double-layer drops showed $T_c = (11.84 \pm 0.34)$ μm and $T_e = (12.52 \pm 0.34)$ μm.

Films of THV 20 wt% in 50–50 vol% MIBK–acetone were ink-jet printed using a drop spacing of 600 μm, corresponding to a 50% of overlapping. The printed films did not show the coffee ring effect,

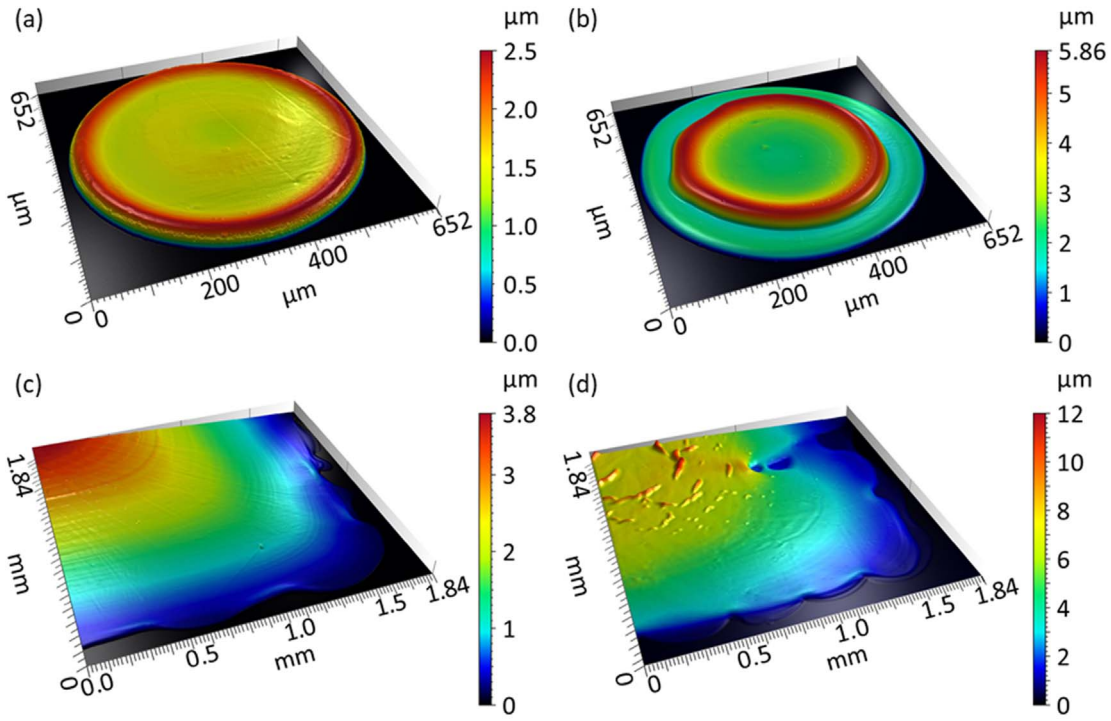

Figure 6. Surface topography corresponding to (a) a one-layer drop, (b) a two-layer drop, (c) a one-layer film and (d) a two-layer film of ink-jet printed THV 10 wt% in MIBK.

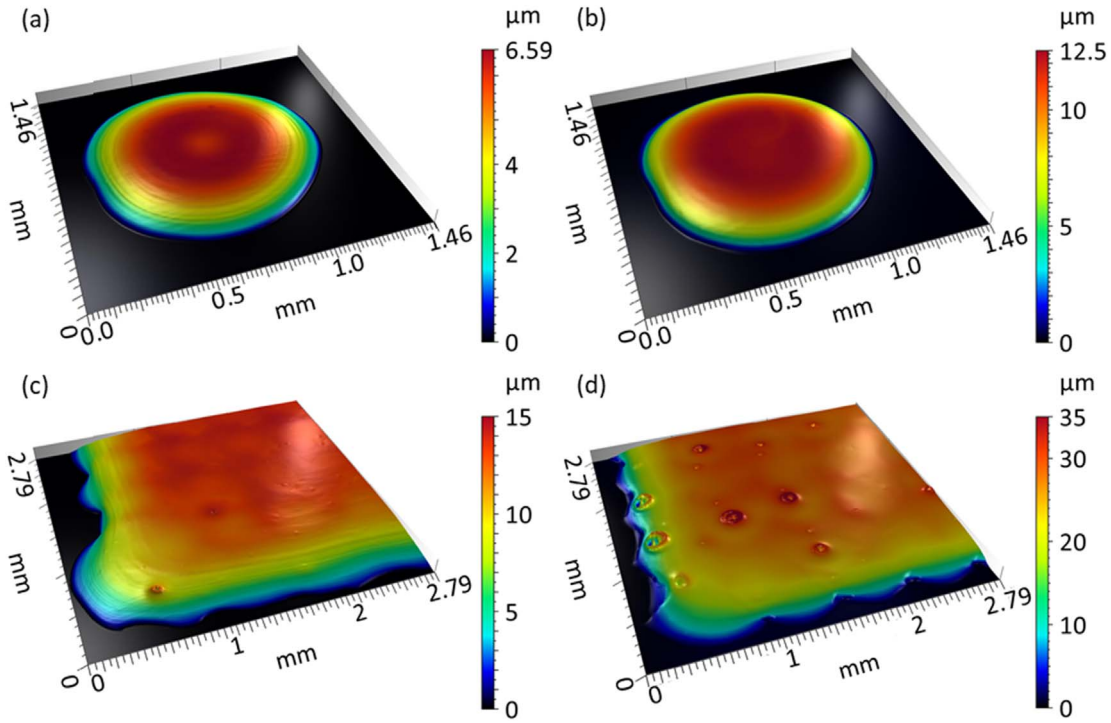

Figure 7. Surface topography corresponding to (a) a one-layer drop, (b) a two-layer drop, (c) a one-layer film and (d) a two-layer film of ink-jet printed THV 20 wt% in MIBK–acetone.

instead, a slipping pattern was present (see figures 7(c), (d)), similarly to the case when THV 10 wt% in MIBK was used to print films. Single-layer films had $T_c = (14.04 \pm 0.52)$ μm, showing a smooth texture with $Sq = (53 \pm 7)$ nm, while double-layer films had $T_c = (28.01 \pm 0.11)$ μm and $Sq = (422 \pm 97)$ nm. Sq was calculated over an area of (1×1) mm at the centre of the films.

Unlike the case when the THV 10 wt% in MIBK ink was used, double-layer films of THV 20 wt% in

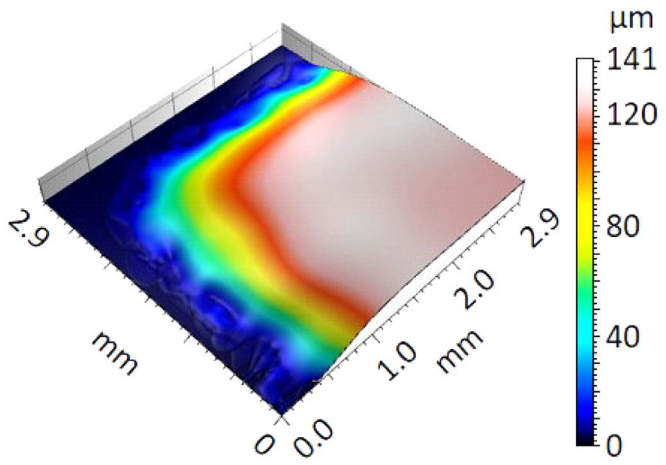

Figure 8. Surface topography corresponding to a heat-treated ten-layer film of ink-jet printed THV 20 wt% in MIBK–acetone.

50–50 vol% MIBK–acetone did not show the formation of wrinkle-like features, instead, the surface topography maps revealed the presence of local cone-shape features, likely caused by the swelling of regions of the previous THV layer during evaporation. Acetone has a faster dissolution rate for THV than MIBK, meaning that less regions would be insufficiently dissolved and, therefore, minimising the formation of wrinkles.

Defects on the surface of multi-layer films can be corrected by subjecting the sample to a heat treatment in a subsequent step. After being heated in an oven at 170 °C for 40 min, a ten-layer film with $T_c = (138 \pm 2.35)\ \mu$m showed a smooth texture with $Sq = (47 \pm 6)$ nm (see figure 8). The latter Sq value is similar to the single-layer result.

4. Conclusion

This study showed that THV can be ink-jet printed at low and high polymer concentrations, from 1 wt% to 20 wt%, to produce protective layers or membranes with thickness of a few nanometres to several micrometres, which may be used to encapsulate drugs and manufacture microfluidic devices. Ink-jet printing of THV also has the potential to be applied to the fabrication of micro-channels used in biochips or lab-on-a-chip devices to mix, pump, or control a biochemical environment. The combination of different printers could allow for both high throughput and high resolution.

We have demonstrated solutions to minimise the coffee ring effect and the formation of wrinkle-like features on the surface when ink-jet printing THV, which should allow the production of films with uniform thickness and surface texture. One way to supress the coffee ring effect when ink-jet printing THV is to increase the polymer concentration, which consequently increases the viscosity of the ink. A high viscosity slows down the diffusion of particles towards the edges by moderating the outward capillary flow [46]. The latter effect allowed a more even distribution of the solute, as the edges of the drop or film kept receding during evaporation. An alternative way to counter the coffee ring effect and the formation of wrinkle-like features on the surface when ink-jet printing THV is to change the evaporation profile of the ink by using a combination of solvents, as the coffee ring effect is caused by the higher evaporation rate at the edge of the drop or film.

CSI offers sub-nanometre precision along the direction of surface height and sub-micrometre lateral resolution areal surface topography measurement of ink-jet printed transparent polymer parts without any potential damage to the surface. The acquired surface information is essential for providing feedback to the manufacturing process and for quality control of the product.

Acknowledgments

This work was supported by the Engineering and Physical Sciences Research Council (EPSRC) (Grants EP/M008983/1, EP/L01534X/1), the European Union's Horizon 2020 Research and Innovation Programme (MNR4SCell, 734174) and the Mexican National Council of Science and Technology (CONACYT) (Reference 600454/438270).

ORCID iDs

Carlos Gomez https://orcid.org/0000-0001-8897-8895

References

[1] ISO/ASTM 52900:2015 2015 *Additive manufacturing—General Principles—Terminology* (Geneva: International Organization for Standardization)
[2] Gibson I, Rosen D W and Stucker B 2015 *Additive Manufacturing Technologies: Rapid Prototyping to Direct Digital Manufacturing* (New York: Springer)
[3] Wohlers T 2018 *Wohlers Report 2018* (Fort Collins: Wohlers Associates)

[4] Guo Y, Patanwala H S, Bognet B and Ma A W K 2017 Inkjet and inkjet-based 3D printing: connecting fluid properties and printing performance *Rapid Prototyping Journal* **23** 562–76
[5] Tekin E, de Gans B and Schubert U 2004 Ink-jet printing of polymers—from single dots to thin film libraries *Journal of Materials Chemistry* **14** 2627–32
[6] Leach R K, Bourell D, Carmignato S, Donmez A, Senin N and Dewulf W 2019 Geometrical metrology for metal additive manufacturing *CIRP Annals* **68** 677–700
[7] Senin N, Thompson A and Leach R K 2017 Feature-based characterisation of signature topography in laser powder bed fusion of metals *Measurement Science and Technology* **29** 045009
[8] de Pastre M A, Thompson A, Quinsat Y, Albajez J A, Senin N and Leach R K 2020 Polymer powder bed fusion surface texture measurement *Measurement Science and Technology* **31** 055002
[9] Smith D W, Iacono S T and Iyer S S 2014 *Handbook of Fluoropolymer Science and Technology* (Hoboken, NJ: Wiley)
[10] Wiley-VCH 2016 *Ullmann's Polymers and Plastics: Products and Processes* (Weinheim: Wiley-VCH)
[11] Ok S, Sadaf S and Walder L 2014 Basic characterization and investigation of a fluorinated terpolymer in pure state and in mixtures with kaolinite at solid interphases of thin films prepared by facile solution cast and nonsolvent methods *High Performance Polymers* **26** 779–89
[12] Ameduri B and Boutevin B 2004 *Well-Architectured Fluoropolymers: Synthesis, Properties and Applications* (Amsterdam: Elsevier)
[13] Drobny J G 2008 *Technology of Fluoropolymers* (Boca Raton: CRC Press)
[14] Gardiner J 2015 Fluoropolymers: origin, production, and industrial and commercial applications *Australian Journal of Chemistry* **68** 13–22
[15] Ok S, Furquan S A, Khan Z and Dogan A U 2016 Near superhydrophobic-fluorinated THV fiber-like structures and fibers prepared by electrospinning *High Performance Polymers* **28** 206–14
[16] Pacetti S 2008 Use of a terpolymer of tetrafluoroethylene, hexafluoropropylene, and vinylidene fluoride in drug eluting coatings on medical devices US 2008/0118541 A1Issuing country: San Jose, CA (USA) Patent publication number
[17] Begolo S, Colas G, Viovy J L and Malaquin L 2011 New family of fluorinated polymer chips for droplet and organic solvent microfluidics *Lab on a Chip* **11** 508–12
[18] Slim C, Ratajovà E, Griveau S, Kanoufi F, Ferraro D, Perréard C, d'Orlyé F, Varenne A and Bedioui F 2015 Two-step local functionalization of fluoropolymer Dyneon THV microfluidic materials by scanning electrochemical microscopy combined to click reaction *Electrochemistry Communications* **60** 5–8
[19] Hutchings I M and Martin G D 2012 *Inkjet Technology for Digital Fabrication* (New York: Wiley) 2012
[20] Haque R I, Vié R, Germainy M, Valbin L, Benaben P and Boddaert X 2015 Inkjet printing of high molecular weight PVDF-TrFE for flexible electronics *Flexible and Printed Electronics* **1** 15001
[21] Thuau D, Kallitsis K, Dos Santos F D and Hadziioannou G 2017 All inkjet-printed piezoelectric electronic devices: energy generators, sensors and actuators *Journal of Materials Chemistry* C **5** 9963–6
[22] Fujifilm 2019 Dimatix Materials Printer DMP-2850 Data Sheet, Manufacturer: Fujifilm
[23] Nordson E F D 2018 *PICO Pμlse Data Sheet,* Manufacturer: Nordson EFD,
[24] Smallwood I M 1996 Smallwood I M 1996 Handbook of organic solvent properties (New York: Butterworth-Heinemann)
[25] Gomez C, Su R, de Groot P and Leach R K 2020 Noise reduction in coherence scanning interferometry for surface topography measurement *Nanomanufacturing and Metrology* **3** 68–76
[26] de Groot P 2011 Coherence scanning interferometry ed R K Leach *Optical Measurement of Surface Topography* (Berlin: Springer) pp 187–208
[27] ISO 25178-604: 2013 2013 *Geometrical Product Specification (GPS)—Surface Texture: Areal—part 604: Nominal Characteristics of Non-Contact (Coherence Scanning Interferometry) Instruments* (Geneva: International Organization for Standardization)
[28] de Groot P 2015 Principles of interference microscopy for the measurement of surface topography *Advances in Optics and Photonics* **7** 1–65
[29] Schmit J 2013 White-light interference 3D microscopes ed K Harding *Handbook of optical Dimensional Metrology* (Boca Raton: Taylor & Francis) pp 395–418
[30] Gomez C, Su R, Thompson A, DiSciacca J, Lawes S and Leach R K 2017 Optimization of surface measurement for metal additive manufacturing using coherence scanning interferometry *Optical Engineering* **56** 111714
[31] Fay M F and Dresel T 2017 Applications of model-based transparent surface films analysis using coherence-scanning interferometry *Optical Engineering* **56** 111709
[32] Feng X, Senin N, Su R, Ramasamy S and Leach R K 2019 Optical measurement of surface topographies with transparent coatings *Optics and Lasers in Engineering* **121** 261–70
[33] Sandler N, Kassamakov I, Ehlers H, Genina N, Ylitalo T and Haeggstrom E 2015 Rapid interferometric imaging of printed drug laden multilayer structures *Scientific Reports* **4** 4020
[34] Goustouridis D, Manoli K, Chatzandroulis S, Sanopoulou M and Raptis I 2005 Characterization of polymer layers for silicon micromachined bilayer chemical sensors using white light interferometry *Sensors and Actuators B: Chemical* **111–112** 549–54
[35] Launhardt M, Woerz A, Loderer A, Laumer T, Drummer D, Hausotte T and Schmidt M M 2016 Detecting surface roughness on SLS parts with various measuring techniques *Polymer Testing* **53** 217–26
[36] de Groot P 2017 The meaning and measure of vertical resolution in optical surface topography measurement *Applied Sciences* **7** 54
[37] Fay M, de Lega X C, de Groot P and OSA Technical Digest 2014 Measuring high-slope and super-smooth optics with high-dynamic-range coherence scanning interferometry *Classical Optics* (online), in Optical Fabrication and Testing (OF&T), Classical Optics 2014,OSA Technical Digest, paper OW1B.3
[38] Digital Surf 2017 Digital Surf MountainsMap Software
[39] ISO 25178-2:2012 2012 *Geometrical Product Specifications (GPS) — Surface Texture: Areal — part 2: Terms, Definitions and Surface Texture Parameters* (Geneva: International Organization for Standardization)
[40] ISO 16610-61: 2015 2015 *Geometrical Product Specification (GPS) — Filtration — Part 61: linear Areal Filters — Gaussian Filters* (Geneva: International Organization for Standardization)
[41] Deegan R D 2000 Pattern formation in drying drops *Physical Review* E **61** 475–85
[42] Kuang M, Wang L and Song Y 2014 Controllable printing droplets for high-resolution patterns *Advanced Materials* **26** 6950–8
[43] Xue L and Han Y 2012 Inhibition of dewetting of thin polymer films *Progress in Material Science* **57** 947–79
[44] Okuzono T, Ozawa K and Doi M 2006 Simple model of skin formation caused by solvent evaporation in polymer solutions *Physical Review Letters* **97** 136103
[45] Baldwin K A and Fairhurst D J 2014 The effects of molecular weight, evaporation rate and polymer concentration on pillar formation in drying poly(ethylene oxide) droplets *Colloids and Surfaces A: Physicochemical and Engineering Aspects* **441** 867–71
[46] Li Y, Yang Q, Li M and Song Y 2016 Rate-dependent interface capture beyond the coffee-ring effect *Scientific Reports* **6** 24628